

# Symmetries and collective excitations in large superconducting circuits

David G. Ferguson,<sup>1</sup> A. A. Houck,<sup>2</sup> and Jens Koch<sup>1</sup>

<sup>1</sup>*Department of Physics & Astronomy, Northwestern University, Evanston, IL 60208, USA*

<sup>2</sup>*Department of Electrical Engineering, Princeton University, Princeton, NJ 08544, USA*

(Dated: August 29, 2012)

The intriguing appeal of circuits lies in their modularity and ease of fabrication. Based on a toolbox of simple building blocks, circuits present a powerful framework for achieving new functionality by combining circuit elements into larger networks. It is an open question to what degree modularity also holds for quantum circuits – circuits made of superconducting material, in which electric voltages and currents are governed by the laws of quantum physics. If realizable, quantum coherence in larger circuit networks has great potential for advances in quantum information processing including topological protection from decoherence. Here, we present theory suitable for quantitative modeling of such large circuits and discuss its application to the fluxonium device. Our approach makes use of approximate symmetries exhibited by the circuit, and enables us to obtain new predictions for the energy spectrum of the fluxonium device which can be tested with current experimental technology.

In the search for a viable architecture for solid-state quantum information processing, superconducting circuits have been the focus of immense interest<sup>1–4</sup>. While research efforts have led to the remarkable improvement of coherence times by nearly 5 orders of magnitudes<sup>5</sup> relative to those in the pioneering experiments a decade ago<sup>6,7</sup>, superconducting circuits have remained extremely simple – especially when compared to circuits found in commonplace electronic devices. Whether phase, flux, or charge qubits, most superconducting circuits consist of less than a handful of circuit elements.

Experiments with the fluxonium device – a superconducting circuit with more than 40 Josephson junctions – have shown that a larger number of Josephson junctions, and hence degrees of freedom, is not necessarily penalized by reduced coherence times<sup>8,9</sup>. Experimental studies of linear Josephson junction arrays have advanced at a rapid pace<sup>10–16</sup>. However, despite considerable theoretical work<sup>17–27</sup> methods for detailed modeling of larger circuit networks are needed to successfully chart the future territory of quantum coherence in networks of increasing size to, e.g., further explore the possibility of topological protection from decoherence<sup>28–31</sup>. The description presents a considerable challenge to theory due to the combination of several factors: the non-linearity induced by Josephson junctions, the increased number of low energy degrees of freedom, and the peculiar interactions between them induced by flux quantization. As a key step for mastering these difficulties, we here present theory for the fluxonium device starting from its complete degrees of freedom. We demonstrate that circuit symmetries play a crucial role in the organization of the excitation spectrum and, employing the relevant collective modes and their approximate decoupling<sup>26</sup>, we obtain a systematic approximation scheme.

Non-linearity, interactions and a large number of degrees of freedom are challenges commonly encountered in the study of many-electron atoms. Our symmetry based approach resembles methods familiar from atomic and molecular physics where the weak breaking of symmetries leads to the well-known lifting of degeneracies in the fine and hyperfine structure of spectra<sup>32</sup>. For the fluxonium circuit, we demonstrate that approximate symmetry under the unitary group and under permutations of junction variables divide the excitation

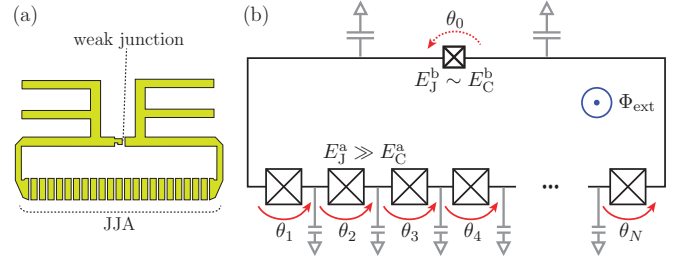


FIG. 1: Circuit of the Fluxonium device: Josephson junction array of nominally identical junctions with Josephson energy  $E_J^a$  and charging energy  $E_C^a$ , shunting one weaker (Josephson and charging energy  $E_J^b$  and  $E_C^b$ , respectively).

spectrum into nearly degenerate subspaces. For realistic parameters, the careful study of perturbations allows us to refine our description and provide new predictions for the collective excitations of the circuit.

## I. FLUXONIUM CIRCUIT

The fluxonium device<sup>8</sup> (Fig. 1) consists of a Josephson junction array with a large number  $N \gg 1$  of nominally identical tunneling junctions. One additional smaller junction (the “black sheep”) shunts the array. The superconducting loop formed this way can be biased with an external magnetic flux  $\Phi_{\text{ext}}$ , making the energy spectrum tunable. As typical of superconducting circuits, the nature of eigenstates and their detailed energy spectrum are governed by the competition between charge transfer across junctions due to Cooper pair tunneling and charging effects due to excess electric charge on individual islands. While the former favors charge delocalization and definite phase differences across each junction, the latter promotes charge localization with definite Cooper pair numbers on each superconducting island. The ratio of Josephson energy ( $E_J$ ) to charging energy ( $E_C$ ) of the involved junctions quantifies this interplay. We use superscripts “a” and “b” in the following to distinguish between array ( $E_J^a/E_C^a \gg 1$ ) and black-sheep parameters ( $E_J^b \sim E_C^b$ ).

The energy spectrum and corresponding eigenstates of the

superconducting circuit  $\mathcal{C}$  are governed by the stationary Schrödinger equation  $H_{\mathcal{C}}|\psi\rangle = E|\psi\rangle$ , in which the circuit Hamiltonian is obtained from the Lagrangian  $\mathcal{L} = T - U$  by circuit quantization<sup>33,34</sup>. For each junction, Josephson tunneling produces a potential energy term  $U_m = -E_{Jm} \cos \theta_m$  where  $\theta_m$  denotes the phase difference across junction  $m$ . The dominant kinetic energy contributions arise from the charging of junction capacitances,  $T_m = \frac{1}{2}C_{Jm}V_{Jm}^2$ , where the voltage drop across junction  $m$  is linked to  $\dot{\theta}_m$  via Josephson's phase evolution equation  $\dot{\theta}_m = 2\pi V_{Jm}/\Phi_0$  and charging energies are related to capacitances via  $E_C = e^2/2C$ .

Fluxoid quantization<sup>35–37</sup> forces the total magnetic flux through the loop to be quantized in units of the superconducting flux quantum  $\Phi_0$ . This leads to the constraint  $\sum_{m=0}^N \theta_m + \varphi_{\text{ext}} = 2\pi z$  where  $\varphi_{\text{ext}} = 2\pi\Phi_{\text{ext}}/\Phi_0$  is the phase offset due to external magnetic flux and  $z$  is an integer. The constraint reduces the number of independent coordinates by one and induces coupling among the remaining degrees of freedom. To incorporate the constraint while maintaining symmetry among array junctions, we eliminate the black-sheep variable  $\theta_0$  and obtain the Lagrangian

$$\mathcal{L} = \frac{\hbar^2}{16E_C^a} \sum_m \dot{\theta}_m^2 + \frac{\hbar^2}{16E_C^b} \left[ \sum_m \dot{\theta}_m \right]^2 + \frac{1}{2} \sum_{mn} \mathcal{G}_{mn} \dot{\theta}_m \dot{\theta}_n - \sum_m E_{Jm}^a \cos \theta_m - E_J^b \cos \left( \sum_m \theta_m + \varphi_{\text{ext}} \right), \quad (1)$$

where, as a convention, sums over Latin indices always run over the range  $1, \dots, N$ . The capacitive term involving the matrix  $\mathcal{G}$  describes the effects from capacitances between superconducting islands and ground (see Supplementary Material).

To illustrate the content of equation (1), it is instructive to note that  $\mathcal{L}$  describes a single fictitious particle inside a periodic potential, albeit in  $N$ -dimensional space with  $N \gg 1$ . Alternatively, it can be interpreted as a description of  $N$  distinguishable particles, each moving in a 1d periodic potential but subject to a peculiar interaction of collective type induced by flux quantization.

The central idea of our approach in the following is to harness the large amount of symmetry present in the dominant terms of equation (1)<sup>43</sup>. In particular, if ground capacitances are negligible and if all array junctions possess the same charging energy  $E_C^a$  and Josephson energy  $E_{J,m}^a = E_J^a$  then  $\mathcal{L}$  is manifestly  $S_N$  symmetric: any permutation  $\sigma \in S_N$  of the array variables leaves the Lagrangian invariant for any value of the external flux. We will refer to this idealization as the Symmetric Fluxonium Model.

In non-relativistic quantum mechanics, such discrete symmetries generally lead to degeneracies which are governed by the irreducible representations of the symmetry group. The simplest irreducible representations of the symmetric group  $S_N$  are the trivial and alternating representations familiar from particle and many-body physics where they dictate the symmetry of wavefunctions for indistinguishable bosons and fermions. In the case of superconducting circuits, degrees of freedom referring to different junctions generally remain dis-

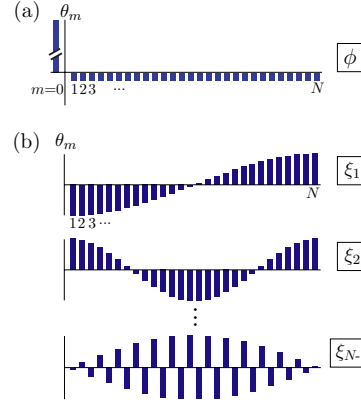


FIG. 2: Normal modes for the  $S_N$  symmetric fluxonium model. Plots show the array variable amplitudes  $\theta_m$  for each normal mode. (a) Superinductance mode  $[\phi]$ , for which all array junction amplitudes  $\theta_m$  are identical. (b) Difference modes  $[\xi_\mu]$ , for all of which the amplitude sum exactly vanishes.

tinguishable, and the full plethora of irreducible representations of  $S_N$  is realized. In this sense, the SFM constitutes an intriguing example of a many-body system with degenerate eigenstates that obey novel permutation symmetries beyond those of bosons and fermions.

## II. $S_N$ SYMMETRIC FLUXONIUM MODEL

From the circuit Lagrangian (1) we now extract the relevant collective modes<sup>26</sup> governing the low-energy physics, and discuss their connection with effective models employed in previous work<sup>8,38</sup>. A key ingredient in the construction of the low-energy modes is the observation that array junctions in fluxonium are dominated by Josephson tunneling,  $E_C^a/E_J^a \ll 1$ , while the black-sheep parameters  $E_C^b$  and  $E_J^b$  are both roughly of the same order as the array charging energy.

For large arrays with junction number  $N \gg E_J^a/E_J^b$ , the potential energy  $U$  exhibits deep minima at positions where all array coordinates have the identical value

$$\theta_m \simeq -\frac{\bar{\varphi}_{\text{ext}} - 2\pi z}{N + E_J^a/E_J^b} \quad (2)$$

with integer  $z$  satisfying  $|z| \ll N$ , and  $\bar{\varphi}_{\text{ext}} = \varphi_{\text{ext}} \bmod 2\pi$ . The minima of  $U$  are surrounded by large energy barriers of height  $\geq 2E_J^a$ , except along the special direction defined by a simultaneous and equal change in all variables, i.e.  $\theta_m = \phi/N$  for all array variables. Such collective dynamics is associated with the black-sheep variable and has a barrier height of only  $2E_J^b$ . In the quantum regime, fluctuations occur primarily along this direction and motivate the use of  $\phi$  as an essential collective variable.

For the Symmetric Fluxonium Model, this collective motion of all array variables forms a normal mode for harmonic fluctuations around the global minimum which, for zero magnetic flux, is located at  $\phi = 0$ . Anticipating the role of this mode we refer to it as the *superinductance mode*. Further analysis shows that the remaining  $N - 1$  normal modes are degenerate and, so as to remain orthogonal to the superinductance mode, their amplitudes sum to zero mode by mode. We therefore call them *difference modes* and introduce  $\xi_\mu$  ( $\mu = 1, \dots, N-1$ ) for their variables (Fig. 2). The transformation to the new set of variables  $\{\phi, \xi_1, \dots, \xi_{N-1}\}$  is facilitated

by

$$\theta_m = \phi/N + \sum_{\mu} W_{\mu m} \xi_{\mu}, \quad (3)$$

and inversely,  $\phi = \sum_m \theta_m$  and  $\xi_{\mu} = \sum_m W_{\mu m} \theta_m$ . Unless otherwise specified sums over Greek-alphabet indices run over the difference modes  $\mu = 1, \dots, N-1$ . Here,  $W$  is a  $(N-1) \times N$  semi-orthogonal matrix with components summing up to zero in each row,  $\sum_m W_{\mu m} W_{\nu m} = \delta_{\mu\nu}$  and  $\sum_m W_{\mu m} = 0$ . Our choice

$$W_{\mu m} = \sqrt{2/N} \cos [\pi\mu(m - \frac{1}{2})/N] \quad (4)$$

differs from the choice in Ref.<sup>26</sup> and proves particularly convenient for the subsequent discussion of corrections from ground capacitances [see Eqs. (7) and (10)] which break  $S_N$  symmetry. After this variable transformation, circuit quantization yields the Symmetric Fluxonium Model Hamiltonian

$$H_{\text{SFM}} = -4E_C^b \partial_{\phi}^2 - 4E_C^a \sum_{\mu} \partial_{\xi_{\mu}}^2 - E_J^b \cos(\phi + \varphi_{\text{ext}}) - E_J^a \sum_m \cos \left[ \phi/N + \sum_{\mu} W_{\mu m} \xi_{\mu} \right], \quad (5)$$

where  $E_C^b = E_C^b/[1 + E_C^b/(E_C^a N)]$  is equal to the black-sheep up to a small  $1/N$ -correction.

The structure of  $H_{\text{SFM}}$  illustrates the utility of the collective-mode description: coupling between different modes is limited to potential energy terms. Further, at the relevant potential minima, all difference mode variables vanish,  $\xi_{\mu}=0$ , and the arguments of the array cosines [last line of equation (5)] are of order  $1/N$ . Hence, a Taylor expansion for small arguments can be expected to capture the essential low-energy physics. Keeping terms up to second order in this expansion obtains

$$H_0 = -4E_C^{\text{si}} \partial_{\phi}^2 - E_J^b \cos(\phi + \varphi_{\text{ext}}) + \frac{E_L}{2} \phi^2 + \sum_{\mu} \Omega a_{\mu}^{\dagger} a_{\mu},$$

where  $a_{\mu}^{\dagger} = (\xi_{\mu}/\Delta_{\xi} - \Delta_{\xi} \partial_{\xi_{\mu}})/\sqrt{2}$  is the ladder operator creating an excitation in the  $\mu$ -th difference mode,  $\Delta_{\xi} = (8E_C^a/E_J^a)^{1/4}$  is the oscillator length, and  $\Omega = \sqrt{8E_C^a E_J^a}$  the array junction plasma frequency.

The first three terms in the expression for  $H_0$  reproduce the superinductance model that was successfully used in Refs. 8 and 38. It describes the superinductance mode as the coupled system of the black-sheep junction with capacitive energy  $E_C^{\text{si}} = E_C^b$  and a large superinductance<sup>44</sup>  $L_s = N(\Phi_0/2\pi)^2/E_J^a$  with correspondingly small inductive energy  $E_L = E_J^a/N$ . As the second crucial insight from  $H_0$  we note that, within the harmonic approximation, the symmetry of the circuit has been extended to include arbitrary unitary transformations of the  $N-1$  degenerate difference modes. As the superinductance mode is a scalar under the action of the group  $U(N-1)$  it must *completely decouple* from the difference modes in the harmonic limit. This decoupling explains, in part, the

success of the superinductance model in matching experimental spectra in spite of the presence of the large number of additional degrees of freedom. The concept of symmetry-induced decoupling carries over to more complicated circuits that include linear arrays of Josephson junctions.

### III. WEAK $S_N$ SYMMETRY BREAKING

The models discussed so far obey  $S_N$  symmetry and, at the level of  $H_0$ , also  $U(N-1)$  symmetry in the difference-mode subspace. To go beyond the superinductance model and predict corrections arising from the weak interaction between the superinductance mode and the difference modes, we next consider mechanisms leading to symmetry breaking. We consider the following three mechanisms which are likely the dominant ones in present experimental samples: anharmonicities of the potential energy neglected in the above expansion ( $\delta H_U$ ), disorder in the Josephson energies of individual array junctions ( $\delta H_J$ ), and additional stray capacitances of each superconducting island to ground ( $\delta H_C$ ). We first derive the Hamiltonian expressions for each of these corrections, and discuss their effects on the energy spectrum and eigenstates subsequently.

We start with  $\delta H_U$ , the corrections from anharmonicities exhibited by the periodic potential but neglected in the harmonic approximation employed in  $H_0$ . Considering higher-order terms in the Taylor expansion of  $H_{\text{SFM}} - H_0$ , we find that the leading anharmonic corrections are given by

$$\delta H_U = -\frac{E_J^a}{4!} \sum_m \left( \phi/N + \sum_{\mu} W_{\mu m} \xi_{\mu} \right)^4. \quad (6)$$

It is easy to verify that  $\delta H_U$  breaks the  $U(N-1)$  symmetry but preserves the permutation symmetry under  $S_N$ .

To derive an expression for  $\delta H_J$ , we capture disorder in the Josephson energies of the array by defining  $E_{Jm} = E_J^a + \delta E_{Jm}$ . Such disorder is expected to be caused by slight variations in junction size and thickness, and may also be affected by junction aging. In the absence of experimental statistics for fluxonium junction parameters, we choose random  $\delta E_{Jm}$  from a Gaussian distribution of width  $\delta E_J = 150\text{MHz}$  and, without loss of generality, impose  $\sum_m \delta E_{Jm} = 0$ . The disorder modifies the potential energy of the Hamiltonian, and by Taylor expanding we obtain

$$\delta H_J = \frac{1}{2} \sum_m \delta E_{Jm} \left( \phi/N + \sum_{\mu} W_{\mu m} \xi_{\mu} \right)^2.$$

Disorder in individual array junction parameters generally leads to weak breaking of both  $U(N-1)$  and  $S_N$  symmetry.

To capture corrections from stray capacitances of the superconducting islands to ground, we include the terms due to ground capacitances shown in equation (1). Ground capacitances contribute kinetic energy terms which are easily expressed as  $T_j = \frac{1}{2}(\Phi_0/2\pi)^2 C_{\text{gj}} \dot{\varphi}_j^2$  when using node variables  $\varphi_j$  for each superconducting island. Assuming overall charge neutrality of the circuit, we can recast these additional contributions in terms of the junction variables  $\theta_m$ . Accounting for

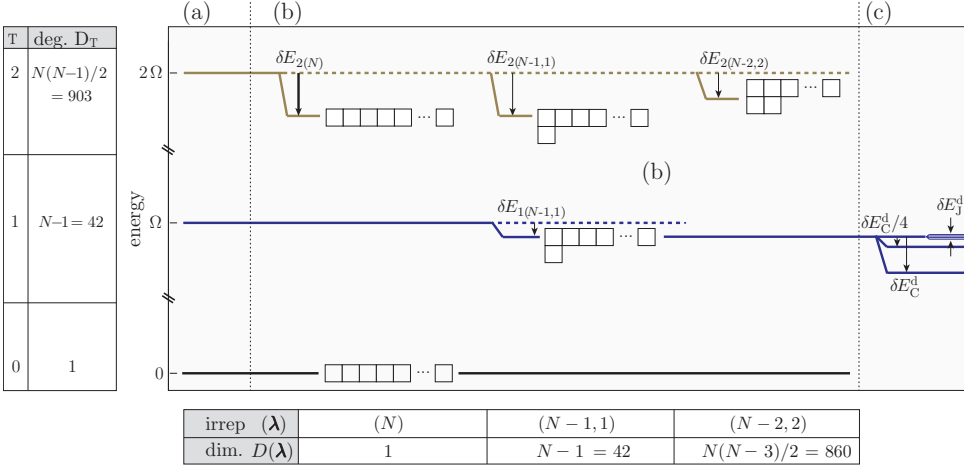


FIG. 3: Difference mode spectrum for total excitation numbers  $T = 0, 1, 2$ . (a) Within the harmonic approximation,  $S_N$  and  $U(N-1)$  symmetry hold and produce degenerate subspaces of dimension  $D_T$ . (b) Anharmonicity  $\delta H_U$  breaks  $U(N-1)$  but leaves  $S_N$  symmetry intact. The irreducible representations of  $S_N$ , labeled by partitions ( $\lambda$ ) or Young diagrams, give rise to  $D(\lambda)$ -dimensional degenerate subspaces. (c) Corrections from disorder in array junction  $E_J$ s and ground capacitances,  $\delta H_C + \delta H_I$  break  $S_N$  symmetry. The degeneracy lifting is shown for the  $T=1$  subspace.

the ground capacitances of the two large superconducting islands surrounding the black sheep and those of the remaining small islands by  $C_g^b$ ,  $C_g^a \ll C_J^a$ ,  $C_J^b$  (Fig. 1), the perturbation can be expressed as

$$\delta H_C \simeq 4 \sum_{\mu, \nu=0}^{N-1} (M^{-1} G M^{-1})_{\mu\nu} \partial_{\xi_\mu} \partial_{\xi_\nu}, \quad (7)$$

where  $\partial_{\xi_0} = \partial_\phi$  and  $\partial_{\xi_\mu} = (a_\mu - a_\mu^\dagger)/(\sqrt{2}\Delta_\xi)$  for  $\mu \geq 1$ . The detailed derivation of equation (7) and analytical expressions for the entries of the matrices  $M$  and  $G$  are provided in the Supplementary Material.

After removing irrelevant global energy shifts, the effects of the perturbations  $\delta H_U$ ,  $\delta H_C$  and  $\delta H_I$  can be organized into three categories according to their action on the superinductance and difference modes. Perturbations may introduce coupling among superinductance states ( $\delta H_\bullet^s$ ), coupling among difference mode states ( $\delta H_\bullet^d$ ), as well as coupling between the two subsystems ( $\delta H_\bullet^{sd}$ ).

We first discuss corrections in the  $\delta H_\bullet^s$  category. The simplest contributions of this type are terms whose structure matches terms already present in  $H_0$ , and hence merely renormalize the superinductance model parameters. Both  $\delta H_U$  and  $\delta H_C$  contain corrections of this type and yield renormalized parameters

$$\begin{aligned} E_C^{\text{si}} &\rightarrow \frac{1}{1/E_C^b + 1/NE_C^a + G_{00}}, \\ E_L &\rightarrow \frac{E_J^a}{N} \left[ 1 - \Delta_\xi^2 \frac{N-1}{4N} \right]. \end{aligned} \quad (8)$$

We emphasize that the inclusion of ground capacitances of the large islands alone leave the  $S_N$  symmetry unharmed and can be completely accounted for in our model by the above renormalization, even in the limit that  $C_g^b$  is large. The only contribution of type  $\delta H_\bullet^s$  which goes beyond renormalization is the term  $-E_J^a \phi^4/(4N^3)$  generated by  $\delta H_U$ . For realistic parameters, we find that this perturbation generates level shifts well below 100MHz (Fig. 4a).

We next turn to corrections in the  $\delta H_\bullet^d$  category with contributions from each  $\delta H_U$ ,  $\delta H_C$  and  $\delta H_I$ . Perturbations like

$\delta H_U$  which do not break the  $S_N$  symmetry, do not lift degeneracies completely and necessitate the use of degenerate perturbation theory. Each remaining degenerate subspace is then associated with an irreducible representation of the symmetric group. Our construction of the relevant irreducible subspaces can be sketched as follows. We start by decomposing the difference-mode Hilbert space into orthogonal subspaces  $\mathcal{V}_T$  with fixed excitation number  $T = \sum_\mu a_\mu^\dagger a_\mu$ , i.e.,  $\mathcal{H}_d = \mathcal{V}_0 \oplus \mathcal{V}_1 \oplus \dots$ . In general, each  $\mathcal{V}_T$  may still be reducible under  $S_N$  and should be decomposed further.

In the decomposition, the integer partitions of  $N$  serve as labels for the irreducible representations of the symmetric group  $S_N$ . Here, a partition  $(\lambda) = (\lambda_1, \lambda_2, \dots, \lambda_F)$  is a sequence of non-increasing positive integers  $\lambda_1 \geq \lambda_2 \geq \dots \geq \lambda_F > 0$  that sum to  $N$ , and are represented by a unique Young diagram. Since the inductive decomposition<sup>39</sup> is not very practical for  $N \gg 1$ , we instead achieve decomposition of  $\mathcal{V}_T$  by using a restricted set of semi-standard Young tableaux<sup>40</sup>. (Technical details of this procedure are provided in the Supplementary Material.) For the low-energy part of the spectrum probed by experiments, we find that the excitation number  $T$  and partition  $(\lambda)$  are sufficient to specify the relevant irreducible subspaces.

The  $T = 0$  subspace, spanned by only the ground state  $|0\rangle$ , immediately forms an irreducible representation. The state is effectively bosonic and is indexed by the partition  $(\lambda) = (N)$ . For  $T = 1$ , likewise,  $\mathcal{V}_1$  already forms an irreducible  $N-1$ -dimensional subspace corresponding to the representation with partition  $(\lambda) = (N-1, 1)$  (Fig. 3). For  $T = 2$  the decomposition is more interesting and results in three irreducible subspaces indexed by  $(N)$ ,  $(N-1, 1)$  and  $(N-2, 2)$ . The subspace labeled by  $(N)$ , for example, is comprised of a

T	(λ)	$-\delta E_U^d[T, (\lambda)]/E_C^a$
0	(N)	0
1	(N-1, 1)	$1 - 1/N$
2	(N)	$3 - 3/N$
2	(N-1, 1)	$3 - 4/N$
2	(N-2, 2)	$2 - 2/N$

TABLE I: Energy corrections for difference mode states due to anharmonicities ( $\delta H_U$ ).  $T$  is the total number of excitations in the difference modes and  $(\lambda)$  the partition labeling the irreducible subspace.

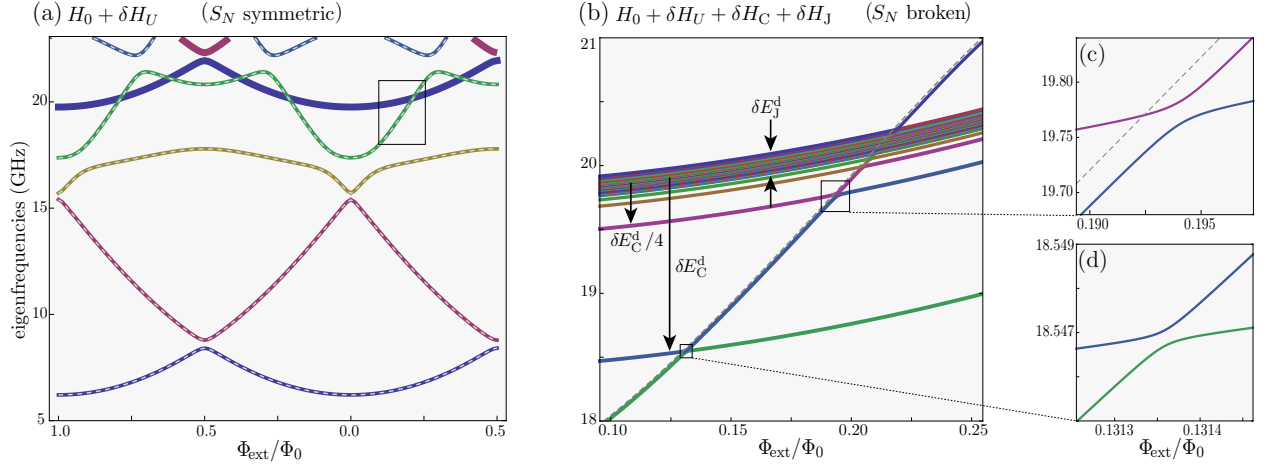


FIG. 4: Spectrum from numerical diagonalization including effects of (a) anharmonicity, and (b) anharmonicity, ground capacitances and junction disorder. Dashed curves show the pure superinductance spectrum for renormalized  $E_C^b$  and  $E_L$  [equation (8)]. Thick curves in (a) indicate  $N - 1$ -fold degenerate levels that remain decoupled from  $\tau = 0$  states under  $\delta H_U$ . (b) Corrections from ground capacitances  $\delta H_C$  and junction disorder  $\delta H_J$  break  $S_N$  symmetry. In the  $\tau = 1$  manifold, ground capacitances split off several levels; smaller shifts are due to junction disorder  $\delta E_{J,\mu}^d$ , here chosen from a Gaussian distribution. The panels in (c), (d) show magnifications of regions marked in (b). The avoided crossing in (c) is primarily generated by ground capacitances. The even smaller splitting in (d) is purely generated by array junction disorder. Parameters are chosen consistent with experimental device (Supplementary Material).

single  $S_N$  invariant state given by

$$|\tau(\lambda)\rangle = |2(N)\rangle = \frac{1}{\sqrt{2(N-1)}} \sum_{\mu} (a_{\mu}^{\dagger})^2 |0\rangle, \quad (9)$$

which is independent of the specific choice of  $W$  in equation (3). By employing perturbation theory for  $\delta H_U^d$  in each irreducible subspace  $\mathcal{V}_{\tau(\lambda)}$ , we obtain the first order energy corrections  $\delta E_{\tau}^d[\tau, (\lambda)]$  in Table I. The resulting level shifts are shown schematically in Fig. 3b.

We next discuss the effects of ground capacitances,  $\delta H_C^d$ , and junction disorder,  $\delta H_J^d$ , on states in the  $1$ -excitation subspace  $\mathcal{V}_1$ . If the ground capacitance of the big islands is sufficiently large compared to that of the small islands,  $E_g^b/E_g^a \ll 1/N^2$ , then  $\delta H_C^d$  in equation (7) is approximately diagonal. This decoupling is the primary motivation for our choice of difference modes (Eq. 3). To leading order, the resulting energy shifts are given by

$$\delta E_{C,\mu}^d \approx -\delta E_C^d/\mu^2 \quad (\mu \ll N), \quad (10)$$

where  $\delta E_C^d = N^2 E_C^{a2}/(\pi^2 \Delta_{\xi} E_g^b)$ . Similar effects from ground capacitances have been predicted and observed in Ref. 16. For higher values of  $\mu$ , shifts induced by Josephson energy disorder  $\delta H_J^d$  become dominant in our model. For Gaussian distributed junction parameters  $\delta E_{J,\mu}$ , the first-order energy shifts  $\delta E_{J,\mu}^d$  also follow a Gaussian distribution with width  $\delta E_J^d = \delta E_J \Delta_{\xi}^2/2$  (Figs. 3c and 4b).

Corrections in the third and final category,  $\delta H_{\bullet}^{\text{sd}}$ , arise from coupling between superinductance and difference modes. Anharmonicity captured by  $\delta H_U^d$  preserves  $S_N$  symmetry and hence, by Schur's lemma, cannot couple states belonging to different irreducible representations. More specifically, states of the form  $|\ell'\rangle \otimes a_{\mu}^{\dagger}|0\rangle$  cannot couple to states of the form

$|\ell\rangle \otimes |0\rangle$  under  $S_N$  symmetry, even when such states are degenerate (Fig. 4a). This symmetry-enforced lack of coupling between the superinductance mode and the lowest difference-mode excitations constitutes the second central result of our work. It is a crucial ingredient in preserving the respective identity of these collective modes and explains the quantitative accuracy of the superinductance model at low energies. The only difference-mode excitations that *may* couple to states of the form  $|\ell'\rangle \otimes |0\rangle$  are those that are bosonic, i.e., are indexed by the partition  $(N)$ . The candidate states with lowest energies are  $|\ell'\rangle \otimes |(N)2\rangle$  but are already well beyond the frequency range probed by spectroscopy in previous fluxonium experiments.

Ground capacitances, as described by  $\delta H_C^{\text{sd}}$ , break  $S_N$  symmetry but preserve “circuit parity”: mirroring of the circuit variables according to  $\varphi_j \rightarrow \varphi_{N-j}$ ,  $\varphi_{\text{ext}} \rightarrow -\varphi_{\text{ext}}$  leaves the Hamiltonian invariant. The superinductance mode and difference modes with odd index  $(\mu + 1)$  are *odd* under parity; difference modes with even index  $(\mu + 1)$  are *even* under parity. As a result,  $\delta H_C^{\text{sd}}$  can only couple the superinductance mode to every other difference mode. We find that the coupling is largest for small values of  $\mu$  and takes the form

$$\delta H_C^{\text{sd}} \approx \partial_{\phi} \sum_{\mu=2,4,6,\dots} \delta E_C^{\text{sd}} (a_{\mu} - a_{\mu}^{\dagger})/\mu^2, \quad (11)$$

where  $\delta E_C^{\text{sd}} = 8 E_C^a E_C^{\text{si}} N^{3/2}/(\pi^2 E_g^b)$ . Finally, all symmetries are broken for array junction disorder, and the resulting perturbation is given by

$$\delta H_J^{\text{sd}} \approx \phi \sum_{\mu} \delta E_{J,\mu}^{\text{sd}} (a_{\mu} + a_{\mu}^{\dagger}), \quad (12)$$

with  $\delta E_{J,\mu}^{\text{sd}}$  following a Gaussian distribution of width  $\delta E_J \Delta_{\xi}/(\sqrt{2}N)$ . As shown in Figs. 4c,d, the coupling between



superinductance and the  $\mu = 1$  difference mode, induced by  $\delta H_J^{\text{sd}}$  only, is considerably smaller than the coupling to the  $\mu = 2$  difference mode which is dominated by  $\delta H_C^{\text{sd}}$ .

#### IV. DISCUSSION AND SUMMARY

Not surprisingly, the low-energy spectrum of the full fluxonium circuit includes, in addition to the energy levels predicted by the superinductance model a large number of nearly degenerate excitations. We have identified the nature of these collective excitations with the difference modes at energies near the array junction plasma frequency. Degeneracies are expected to be lifted, first by  $U(N-1)$  symmetry breaking due to anharmonicity and further by  $S_N$  symmetry breaking due to array junction disorder ground capacitances. The important consequences of these corrections include separation of previously degenerate levels into closely spaced multiplets.

Josephson junction arrays provide an interesting example of a quantum system with many identical but *distinguishable* degrees of freedom, resulting in representations of the symmetric group not readily observed in nature with indistinguishable particles. Invariance under permutations of the junction variables is a generic symmetry expected to be important for any large superconducting circuit containing one or several Josephson junction arrays. The decomposition of the symmetric group  $S_N$  into irreducible representations relevant at low energies thus becomes an important tool in circuit analysis. For the example of the fluxonium device, we have shown that such symmetry strongly restricts the possible cou-

pling between the superinductance mode, as observed in the experiment<sup>8,9</sup>, and the additional difference modes. Our results explain the remarkable accuracy of the effective superinductance model as long as the renormalizations of  $E_L$  and  $E_C^{\text{si}}$  are taken into account, and are consistent with previous fits of experimental data where  $E_L$  and  $E_C^{\text{si}}$  were used as a fit parameters, producing excellent agreement<sup>8,9,41</sup>.

The power of symmetry-based approaches in the analysis of future circuits is easily illustrated for the example of the fluxonium device. Specifically, the number of difference-mode states with excitations up to some threshold  $T$  grows rapidly as  $\frac{(T+N-1)!}{T!(N-1)!}$ . The number of states with proper bosonic symmetry, however, is dramatically smaller: For  $N = 43$  and  $T = 5$  there are  $10^6$  difference mode states but merely 6 of them possess bosonic symmetry. Harnessing exact and approximate symmetries of Hamiltonians for larger circuits will likely be a crucial ingredient in future research exploring quantum coherence in superconducting circuit networks of increasing complexity.

#### Acknowledgments

We thank Leonid Glazman, Michel Devoret and Vladimir Manucharyan for stimulating discussions. Our research was supported by the NSF under Grants PHY-1055993 (JK, DGF), DMR-0805277 (DGF), and by the David and Lucile Packard Foundation (AAH).

- 
- <sup>1</sup> Makhlin, Y., Schön, G. & Shnirman, A., Quantum-state engineering with Josephson-junction devices. *Rev. Mod. Phys.* **73**, 357 (2001).
  - <sup>2</sup> Devoret, M. H. & Martinis, J. M., Implementing qubits with superconducting integrated circuits. *Quantum Inf. Process.* **3**, 163–203 (2004).
  - <sup>3</sup> Schoelkopf, R. J. & Girvin, S. M., Wiring up quantum systems. *Nature* **451**, 664–669 (2008).
  - <sup>4</sup> Clarke, J. & Wilhelm, F. K., Superconducting quantum bits. *Nature* **453**, 1031–1042 (2008).
  - <sup>5</sup> Paik, H. *et al.*, Observation of High Coherence in Josephson Junction Qubits Measured in a Three-Dimensional Circuit QED Architecture. *Phys. Rev. Lett.* **107**, 240501 (2011).
  - <sup>6</sup> Bouchiat, V. *et al.*, Quantum Coherence with a Single Cooper Pair. *Phys. Scr.* **T76**, 165 (1998).
  - <sup>7</sup> Nakamura, Y., Pashkin, Y. A. & Tsai, J. S., Coherent control of macroscopic quantum states in a single-Cooper-pair box. *Nature* **398**, 786–788 (1999).
  - <sup>8</sup> Manucharyan, V. *et al.*, Fluxonium: Single Cooper-Pair Circuit Free of Charge Offsets. *Science* **326**, 113–116 (2009).
  - <sup>9</sup> Manucharyan, V. *et al.*, Evidence for coherent quantum phase-slips across a Josephson junction array. *Phys. Rev. B* **85**, 24521 (2012).
  - <sup>10</sup> Chow, E., Delsing, P. & Haviland, D., Length-Scale Dependence of the Superconductor-to-Insulator Quantum Phase Transition in One Dimension. *Phys. Rev. Lett.* **81**, 204–207 (1998).
  - <sup>11</sup> Haviland, D. B., Andersson, K. & Ågren, P., Superconducting and Insulating Behavior in One-Dimensional Josephson Junction Arrays. *J. Low Temp. Phys.* **118**, 733–749 (2000).
  - <sup>12</sup> Takahide, Y., Miyazaki, H. & Ootuka, Y., Superconductor-insulator crossover in Josephson junction arrays due to reduction from two to one dimension. *Phys. Rev. B* **73**, 224503 (2006).
  - <sup>13</sup> Pop, I. M. *et al.*, Measurement of the current-phase relation in Josephson junction rhombi chains. *Phys. Rev. B* **78**, 104504 (2008).
  - <sup>14</sup> Pop, I. M. *et al.*, Measurement of the effect of quantum phase slips in a Josephson junction chain. *Nature Phys.* **6**, 589–592 (2010).
  - <sup>15</sup> Bell, M. T. *et al.*, Superinductor with Tunable Non-Linearity. arXiv:1206.0307 (2012).
  - <sup>16</sup> Masluk, N. A. *et al.*, Implementation of low-loss superinductances for quantum circuits. arXiv:1206.2964 (2012).
  - <sup>17</sup> Bradley, R. M. & Doniach, S., Quantum fluctuations in chains Josephson junctions. *Phys. Rev. B* **30**, 1138 (1984).
  - <sup>18</sup> Choi, M. Y., Persistent current and voltage in a ring of Josephson junctions. *Phys. Rev. B* **48**, 15920 (1993).
  - <sup>19</sup> Hermon, Z., Ben-Jacob, E. & Schön, G., Charge solitons in one-dimensional arrays of serially coupled Josephson junctions. *Phys. Rev. B* **54**, 1234–1245 (1996).
  - <sup>20</sup> Odintsov, A., One-dimensional Josephson arrays as superlattices for single Cooper pairs. *Phys. Rev. B* **54**, 1228–1233 (1996).
  - <sup>21</sup> Glazman, L. & Larkin, A., New Quantum Phase in a One-Dimensional Josephson Array. *Phys. Rev. Lett.* **79**, 3736–3739 (1997).
  - <sup>22</sup> Choi, M.-S. *et al.*, Quantum phase transitions in Josephson-junction chains. *Physical Review B* **57**, R716–R719 (1998).
  - <sup>23</sup> Matveev, K. A., Larkin, A. I. & Glazman, L. I., Persistent current

- in superconducting nanorings. *Phys. Rev. Lett.* **89**, 96802 (2002).
- <sup>24</sup> Goswami, P. & Chakravarty, S., Dissipation, topology, and quantum phase transition in a one-dimensional Josephson junction array. *Phys. Rev. B* **73**, 094516 (2006).
  - <sup>25</sup> Homfeld, J. *et al.*, Charge solitons and their dynamical mass in one-dimensional arrays of Josephson junctions. *Phys. Rev. B* **83** (2011).
  - <sup>26</sup> Catelani, G. *et al.*, Relaxation and frequency shifts induced by quasiparticles in superconducting qubits. *Phys. Rev. B* **84** (2011).
  - <sup>27</sup> Rastelli, G. *et al.*, Quantum phase-slips in Josephson junction chains: effects of finite size and propagating modes. arXiv:1201.0539 (2012).
  - <sup>28</sup> Ioffe, L. B. *et al.*, Topologically protected quantum bits using Josephson junction arrays. *Nature* **415**, 503–506 (2002).
  - <sup>29</sup> Kitaev, A., Protected qubit based on a superconducting current mirror. arXiv:cond-mat/0609441 (2006).
  - <sup>30</sup> Gladchenko, S. *et al.*, Superconducting nanocircuits for topologically protected qubits. *Nature Phys.* **5**, 48–53 (2008).
  - <sup>31</sup> Douçot, B. & Ioffe, L. B., Physical implementation of protected qubits. *Rep. Prog. Phys.* **75**, 072001 (2012).
  - <sup>32</sup> Condon, E. U. & Shortley, G. H., *The Theory of Atomic Spectra*, (Cambridge University Press, 1935).
  - <sup>33</sup> Devoret, M. H., Quantum fluctuations in electrical circuits. *Les Houches, Session LXIII* (Elsevier, 1995).
  - <sup>34</sup> Burkard, G., Koch, R. H. & DiVincenzo, D. P., Multilevel quantum description of decoherence in superconducting qubits. *Phys. Rev. B* **69**, 64503 (2004).
  - <sup>35</sup> London, F., *Superfluids, vol. I*, 152, (John Wiley & Sons, New York, 1950).
  - <sup>36</sup> Doll, R. & Näbauer, M., Experimental Proof of Magnetic Flux Quantization in a Superconducting Ring. *Phys. Rev. Lett.* **7**, 51–52 (1961).
  - <sup>37</sup> Deaver, B. & Fairbank, W., Experimental Evidence for Quantized Flux in Superconducting Cylinders. *Phys. Rev. Lett.* **7**, 43–46 (1961).
  - <sup>38</sup> Koch, J. *et al.*, Charging Effects in the Inductively Shunted Josephson Junction. *Phys. Rev. Lett.* **103**, 217004 (2009).
  - <sup>39</sup> Hamermesh, M., *Group Theory and Its Application to Physical Problems*, (Dover Publications, 1989).
  - <sup>40</sup> Sagan, B. E., *The Symmetric Group*, (Springer, 2000).
  - <sup>41</sup> Manucharyan, V. *et al.*, Coherent oscillations between classically separable quantum states of a superconducting loop. arXiv:0910.3039 (2009).
  - <sup>42</sup> Ivanov, D. *et al.*, Interference effects in isolated Josephson junction arrays with geometric symmetries. *Phys. Rev. B* **65**, 024509 (2001).
  - <sup>43</sup> Ref. 42 analyzed the dihedral symmetry of a ring of four identical Josephson junctions with zero or  $\pi$  external flux. However, in Eq. (1) discrete rotational symmetry is broken due to the weak junction.
  - <sup>44</sup> Term introduced by A. Kitaev (unpublished).

## Supplementary Material

### Appendix A: Irreducible representations for difference modes

In this appendix we discuss the decomposition of the difference-mode Hilbert spaces  $\mathcal{V}_T$  into subspaces that transform irreducibly under  $S_N$  symmetry. Since some of the mathematical tools employed may not belong to the physicist's ordinary repertoire, we provide definitions along with concrete examples where appropriate. In terminology and notation, our discussion closely follows, the excellent book by Sagan<sup>40</sup>.

The subspace  $\mathcal{V}_T$  comprises all difference-mode states with total excitation number  $T$ . It is spanned by the orthogonal states

$$a_{\mu_1}^\dagger \cdots a_{\mu_T}^\dagger |0\rangle \quad (\text{A1})$$

where we assume weakly ordered mode indices

$$\mu_1 \leq \cdots \leq \mu_T \in \{1, 2, \dots, N-1\}$$

to avoid double counting. The  $S_N$  symmetry displayed in the ideal fluxonium circuit pertains to permutations  $\sigma \in S_N$  of the array junction variables  $\theta_1, \theta_2, \dots, \theta_N$ . Such permutations also induce linear transformations in the operator space  $\mathbb{C}\{a_1^\dagger, a_2^\dagger, \dots, a_{N-1}^\dagger\}$  spanned by the difference-mode creation operators. To understand how  $a_\mu^\dagger$  transforms under permutations, we recall the definition of the creation operators in terms of junction variables:

$$a_\mu^\dagger = \sum_m W_{\mu m} (\theta_m / \Delta_\xi - \Delta_\xi \partial_{\theta_m}) / \sqrt{2}. \quad (\text{A2})$$

Using the identity  $\sum_\mu W_{\mu m} W_{\mu n} = \delta_{mn} - \frac{1}{N}$ , one finds that the difference-mode creation operators transform according to

$$\sigma(a_\mu^\dagger) = \sum_\nu S(\sigma)_{\mu\nu} a_\nu^\dagger. \quad (\text{A3})$$

We remind the reader that, by our convention, sums with Latin (Greek) summation indices always range from 1 to  $N$  (1 to  $N-1$ ). The  $(N-1) \times (N-1)$  transformation matrices are given by

$$S(\sigma)_{\mu\nu} = \sum_{m,n} W_{\mu m} W_{\nu n} D(\sigma)_{mn}. \quad (\text{A4})$$

Here,  $D(\sigma)_{mn} = \delta_{m, \sigma(n)}$  denotes the  $N \times N$  permutation matrix for the group element  $\sigma \in S_N$ . (The matrices  $D(\sigma)$  form the defining representation of  $S_N$ .)

By the relation  $\mathcal{V}_1 = \mathbb{C}\{a_1^\dagger, a_2^\dagger, \dots, a_{N-1}^\dagger\}|0\rangle$ , the transformation matrices  $S(\sigma)$  in equation (A3) define an orthogonal  $S_N$  representation of degree  $N-1$  in the one-excitation subspace. Similarly, for higher excitation numbers  $T > 1$ , the group action for products of creation operators,

$$\sigma(a_{\mu_1}^\dagger \cdots a_{\mu_T}^\dagger) = \sum_{\nu_1, \dots, \nu_T} S(\sigma)_{\mu_1 \nu_1} \cdots S(\sigma)_{\mu_T \nu_T} a_{\nu_1}^\dagger \cdots a_{\nu_T}^\dagger, \quad (\text{A5})$$

determines the representation of  $S_N$  in the subspace  $\mathcal{V}_T$ . Given these representations, our central task is to decompose each  $\mathcal{V}_T$  into its irreducible subspaces. As an aside we note that in the special case of  $\mathcal{V}_1$ , simple arguments based on group characters can be used to show that  $\mathcal{V}_1$  is already irreducible and coincides with the irreducible representation indexed by the partition  $(N-1, 1)$ , for which group characters are known to be  $\text{tr} D(\sigma) - 1$  for arbitrary  $N$  (Ref. 40 section 2.12).

The common approach for decomposition of such product representations is inductive and requires successive decompositions for  $S_1, S_2, \dots, S_N$ , see, e.g., Ref. 39. For large  $N$ , however, that strategy is not very practical. Following the treatment by Sagan<sup>40</sup>, we thus employ an alternate approach using a restricted class of semi-standard tableaux. (We explain the meaning of these words in due course).

As our first step in constructing the decomposition of each  $\mathcal{V}_T$ , we define the pseudo-creators  $b_n^\dagger$  for  $n = 1, 2, \dots, N$  by

$$\begin{aligned} b_n^\dagger &= \sum_\mu W_{\mu n} a_\mu^\dagger \\ &= [(\theta_n - \phi/N) / \Delta_\xi + \Delta_\xi (\partial_{\theta_n} - \partial_\phi)] / \sqrt{2}. \end{aligned} \quad (\text{A6})$$

As one would expect, pseudo-creators  $b_n^\dagger$  increase the total excitation number in the difference-mode subspace by one. The number of pseudo-creators, however, is  $N$  and thus exceeds the number of difference-mode creation operators  $a_\mu^\dagger$  by one. Indeed, the pseudo-creators obey  $\sum_n b_n = 0$  and, hence, are not linearly dependent. They obey the non-standard commutation relation

$$[b_m, b_n^\dagger] = \delta_{mn} - 1/N. \quad (\text{A7})$$

For the price of this anomalous commutator, we obtain operators which transform with elegant simplicity. Specifically, under array variable permutations  $\sigma \in S_N$ , the  $b_n^\dagger$  operators simply undergo permutations:

$$\sigma(b_n^\dagger) = \sum_m D(\sigma)_{nm} b_m^\dagger = b_{\sigma(n)}^\dagger. \quad (\text{A8})$$

This simple transformation law will be crucial for finding the irreducible subspaces of  $\mathcal{V}_T$ .

We next extend the language of difference-mode excitations to pseudo-mode excitations and define the states

$$|\mathbf{t}\rangle = \prod_{n=1}^N (b_n^\dagger)^{t_n} |0\rangle \quad (\text{not normalized}), \quad (\text{A9})$$

where the vector  $\mathbf{t} = (t_1, t_2, \dots, t_N)$  specifies the excitation numbers  $t_n \in \mathbb{N}_0$  for each pseudo-mode  $b_n^\dagger$ . Using the inverse of equation (A6),  $a_\mu^\dagger = \sum_n W_{\mu n} b_n^\dagger$ , it is simple to confirm that

$$\mathcal{V}_T = \text{span}\{|\mathbf{t}\rangle \mid \sum_n t_n = T\}, \quad (\text{A10})$$

i.e., the pseudo-mode excitations span the difference mode subspaces  $\mathcal{V}_T$  one by one.

For a state with given pseudo-mode excitations  $\mathbf{t} = (t_1, t_2, \dots, t_N)$ , equation (A8) implies that  $\sigma \in S_N$  simply permutes the pseudo-mode excitation numbers according to  $\mathbf{t} \rightarrow \mathbf{t}' = (t_{\sigma(1)}, t_{\sigma(2)}, \dots, t_{\sigma(N)})$ .



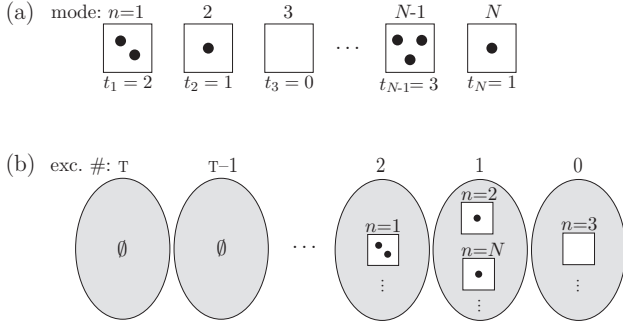


FIG. 5: Labeling schemes for difference mode excitations. (a) Label specifies excitation numbers, mode by mode. (b) Label specifies mode indices, excitation number by excitation number.

*Example:* The state with 3 excitations in pseudo-mode  $n = 1$  and 4 excitations in pseudo-mode  $n = 2$  is  $\mathbf{t} = (3, 4, 0, \dots, 0)$ . A permutation may transform it into  $\mathbf{t}' = (4, 0, 3, 0, \dots, 0)$ , for example but not into  $(2, 5, 0, \dots, 0)$ , even though the latter state still has the same total excitation number  $T = 7$ .

For each state  $|\mathbf{t}\rangle$  with  $T = \sum_n t_n$ , we define the subspace spanned by itself and its permuted partner states:

$$\mathcal{V}_{[\mathbf{t}]} := \text{span} \{ |\mathbf{t}'\rangle = |\sigma\mathbf{t}\rangle \mid \sigma \in S_N \} \subset \mathcal{V}_T, \quad (\text{A11})$$

As suggested by the notation,  $[\mathbf{t}]$  may be understood as an equivalence class when defining  $\mathbf{t} \sim \mathbf{t}' : \Leftrightarrow$  there exists a  $\sigma \in S_N$  such that  $\mathbf{t}' = \sigma\mathbf{t}$ . By construction, the  $\mathcal{V}_{[\mathbf{t}]}$  form  $S_N$ -invariant subspaces, and their unions cover each  $\mathcal{V}_T$

$$\mathcal{V}_T = \bigcup_{\{\mathbf{t} \mid T = \sum_n t_n\}} \mathcal{V}_{[\mathbf{t}]}. \quad (\text{A12})$$

Note that, due to linear dependence of the pseudo-modes, subspaces for inequivalent excitation classes  $[\mathbf{t}] \cap [\mathbf{t}'] = \emptyset$  may, nonetheless, have a non-zero intersection,  $\mathcal{V}_{[\mathbf{t}]} \cap \mathcal{V}_{[\mathbf{t}']} \neq \emptyset$ .

We will first discuss the decomposition of  $\mathcal{V}_{[\mathbf{t}]}$  into irreducible subspaces as if  $b_n$  were orthogonal modes. In step 1, we thus drop the cautionary prefix “pseudo” temporarily and show that the basis vectors  $|\mathbf{t}\rangle$  can then be relabeled in such a way to reveal isomorphism between  $\mathcal{V}_{[\mathbf{t}]}$  and the corresponding permutation module  $M^{\lambda_{\mathbf{t}}}$ . In step 2, we then utilize the important theorem for the decomposition of  $M^{\lambda_{\mathbf{t}}}$  that identifies semi-standard tableaux as the indexing set for all irreducible subspaces. In both steps, we introduce the necessary terminology and explain the construction. We do not provide proofs of the underlying theorems but refer the interested reader to Sagan’s book<sup>40</sup>, chapter 2. Finally, in step 3 we return to the issue of linear dependence of  $b_n$  modes and show how the usual construction can be modified to account for the linear dependence in a simple fashion.

### STEP 1: Isomorphism between $\mathcal{V}_{[\mathbf{t}]}$ and the permutation module $M^{\lambda_{\mathbf{t}}}$

The excitation numbers  $\mathbf{t} = (t_1, t_2, \dots, t_N)$  label each state in  $\mathcal{V}_{[\mathbf{t}]}$  by specifying *excitation numbers, mode by mode*. An alternative labeling scheme (Fig. 5) consists of specifying *mode numbers, excitation level by excitation level*.

To specify the procedure of switching from the first labeling scheme to the second, we define the **partition**  $(\lambda_{\mathbf{t}})$  **associated with**  $\mathbf{t}$  as follows. Consulting  $\mathbf{t}$  and for each integer  $f = 0, 1, \dots, T$ , count

$$\lambda'_f = (\text{number of modes with } f \text{ excitations}). \quad (\text{A13})$$

The resulting sequence  $(\lambda'_0, \lambda'_1, \dots, \lambda'_T)$  sums to  $N$ , the total number of modes. By sorting entries in this sequence in decreasing order and dropping all 0 entries, we obtain the partition  $(\lambda_{\mathbf{t}})$  associated with  $\mathbf{t}$ . Excitation numbers  $\mathbf{t}, \mathbf{t}'$  in the same equivalence class always have the same associated partition.

*Example:* for  $N = 4$  and excitation numbers  $\mathbf{t} = (1, 3, 0, 1)$ , one obtains the sequence  $(1, 2, 0, 1, 0, 0)$  and thus the associated partition  $(\lambda_{\mathbf{t}}) = (2, 1, 1)$ .

The partition  $(\lambda_{\mathbf{t}}) = (\lambda_1, \lambda_2, \dots, \lambda_F)$  is represented by a Young diagram: an array of squares where row  $f$  has  $\lambda_f$  squares. From the Young diagram  $(\lambda_{\mathbf{t}})$  we obtain the **Young tableau**  $\Theta_{\mathbf{t}}$  **associated with**  $\mathbf{t}$  by filling the boxes with the mode indices from 1 to  $N$  in such a way that mode indices with the same excitation number appear in the same row.

*Example:* For  $\mathbf{t} = (1, 3, 0, 1)$ , the Young diagram of  $(\lambda_{\mathbf{t}}) = (2, 1, 1)$  and a Young tableau associated with  $\mathbf{t}$  are given by

$$(\lambda_{\mathbf{t}}) = \begin{array}{|c|c|} \hline \square & \square \\ \hline \square & \\ \hline \square & \\ \hline \end{array} \text{ and } \Theta_{\mathbf{t}} = \begin{array}{|c|c|} \hline \boxed{1} & \boxed{4} \\ \hline \boxed{3} & \boxed{2} \\ \hline \boxed{2} & \\ \hline \end{array}.$$

From the sorting function used to order the entries in the partition  $(\lambda_{\mathbf{t}})$ , one can infer which row in the tableau refers to which excitation number. As a result, the Young tableau lists the mode indices corresponding to each excitation number as intended. One additional modification is required to turn it into the desired state label.

For this, note that the transposition (interchange) of two mode indices with the same excitation number leads to a new tableau (consider interchange of the entries 1 and 4 in our example above) but not to a new state  $|\mathbf{t}\rangle$ . To remove this ambiguity, we define two tableaux as row-equivalent,  $\Theta_{\mathbf{t}} \stackrel{R}{\sim} \Theta'_{\mathbf{t}} : \Leftrightarrow$  permutations of elements within each row can transform  $\Theta'_{\mathbf{t}}$  to  $\Theta_{\mathbf{t}}$ . The resulting equivalence class  $[\Theta_{\mathbf{t}}]$  is called the **tabloid** **associated with**  $\mathbf{t}$  and serves as the new label for each state.

*Example:* Using  $\mathbf{t} = (1, 1, 0, 3)$  as above, the associated tabloid is

$$[\Theta_{\mathbf{t}}] = \left\{ \begin{array}{|c|c|} \hline \boxed{1} & \boxed{4} \\ \hline \boxed{3} & \boxed{2} \\ \hline \boxed{2} & \\ \hline \end{array}, \begin{array}{|c|c|} \hline \boxed{4} & \boxed{1} \\ \hline \boxed{3} & \boxed{2} \\ \hline \boxed{2} & \\ \hline \end{array} \right\}$$

It is useful to note that  $[\Theta_t]$  can also be expressed as  $[\Theta_t] = \{\sigma\Theta_t \mid \sigma \in R\Theta_t\}$  where  $R\Theta_t \subset S_N$  is the subset of permutations which only interchange entries in each row of the tableau  $\Theta_t$ .  $R\Theta_t$  called the row-stabilizer of  $\Theta_t$ . Below, we will also encounter the column-stabilizer  $C\Theta_t$  with the analogous definition referring to columns instead of rows.

With this, we have established a one-to-one map  $|\mathbf{t}\rangle \leftrightarrow |[\Theta_t]\rangle$  which achieves the important goal of relating  $\mathcal{V}_{[\mathbf{t}]}$  to a central object in the representation theory of  $S_N$ : the permutation module  $M^{\lambda_t}$  defined by

$$M^{\lambda_t} = \mathbb{C} \{[\Theta_t] \mid \mathbf{t} \in [\mathbf{t}]\}. \quad (\text{A14})$$

Since each permutation module is defined in terms of tabloids, the group action for  $\mathcal{V}_{[\mathbf{t}]}$  and for  $M^{\lambda_t}$  is easily verified to be identical, and the two vector spaces are hence isomorphic as  $S_N$  representations.

### STEP 2: Decomposing $\mathcal{V}_{[\mathbf{t}]}$ and constructing basis vectors for all irreducible subspaces

The great benefit of identifying  $\mathcal{V}_{[\mathbf{t}]}$  as isomorphic to  $M^{\lambda_t}$  lies in the availability of mathematical tools for decomposing the permutation modules into their irreducible subspaces (see Sagan<sup>40</sup>, section 2.10). For the symmetric group  $S_N$ , each irreducible representation  $S^\mu$  is labeled uniquely by a partition  $(\mu)$  of  $N$ . Consequently, the general decomposition takes the form

$$M^\lambda \cong \bigoplus_{\mu} m_{\mu\lambda} S^\mu, \quad (\text{A15})$$

where  $m_{\mu\lambda} \in \mathbb{N}_0$  is the multiplicity of the irreducible subspace  $S^\mu$  within  $M^\lambda$ . For a given  $\mathcal{V}_{[\mathbf{t}]} \simeq M^{\lambda_t}$ , we wish to obtain the basis vectors for each of the copies (if any) of  $S^\mu$  contained in it. The basis vectors are obtained by means of semi-standard tableaux, which we define next.

The **associated semi-standard tableau**  $\Sigma_t^\mu$  is constructed from the Young diagram for  $(\mu)$  by filling its squares with the excitation numbers  $t_1, t_2, \dots, t_N$  in such a manner that entries in each row weakly increase ( $\leq$ ), and entries in each column strictly increase ( $<$ ). Along with  $\Sigma_t^\mu$ , we consider **standard tableaux**  $\Theta_{st}^\mu$  of the same shape, which is a Young tableau with entries increasing in each row and column. This way, we can set up a lookup function  $\vartheta : \{1, 2, \dots, N\} \rightarrow \{t_1, t_2, \dots, t_N\}$  that extracts the position of the integer  $n$  in the reference tableau  $\Theta_{st}^\mu$  and returns the excitation number entry found in the semi-standard tableau  $\Sigma_t^\mu$  at the corresponding position. To keep notation simple, we usually do not make the dependence of  $\vartheta$  on  $\Sigma_t^\mu$  and  $\Theta_{st}^\mu$  explicit.

*Example:* For  $[\mathbf{t}] = [(0, 1, 0, 3)]$ , the associated semi-standard tableau with shape  $(\mu) = (2, 2)$  and the accompanying reference tableau are:

$$\Sigma_t^\mu = \begin{bmatrix} 0 & 0 \\ 1 & 3 \end{bmatrix}, \quad \Theta_{st}^\mu = \begin{bmatrix} 1 & 3 \\ 2 & 4 \end{bmatrix}.$$

The lookup function then yields the results:

$$\begin{array}{c|cccc} n & 1 & 2 & 3 & 4 \\ \hline \vartheta(n) & 0 & 1 & 0 & 3 \end{array}.$$

With this preparation, one now obtains the basis states spanning the instance(s) of  $S^\mu$  within  $\mathcal{V}_{[\mathbf{t}]}$  from

$$\begin{aligned} & |\Sigma_t^\mu; \Theta_{st}^\mu\rangle \\ &= \sum_{\sigma \in C\Theta_{st}^\mu} \sum_{\tau \in R\Theta_{st}^\mu} \text{sgn}(\sigma)\sigma\tau \left[ b_1^{\dagger\vartheta(1)} b_2^{\dagger\vartheta(2)} \dots b_N^{\dagger\vartheta(N)} \right] |0\rangle \end{aligned} \quad (\text{A16})$$

where permutations  $\sigma, \tau \in S_N$  act on the mode indices, i.e., the subscripts of the  $b_n^\dagger$  operators as before. (Caveat: as defined above, the basis states are not normalized yet.) Each semi-standard tableau  $\Sigma_t^\mu$  yields an irreducible subspace

$$\mathcal{V}_{\Sigma_t^\mu} = \text{span} \{ |\Sigma_t^\mu; \Theta_{st}^\mu\rangle \mid \text{all standard tableaux } \Theta_{st}^\mu \}. \quad (\text{A17})$$

By considering all possible partitions  $(\mu)$  and associated semi-standard tableaux  $\Sigma_t^\mu$ , we thus completely decompose  $\mathcal{V}_{[\mathbf{t}]}$  into linearly independent irreducible subspaces. (The set of partitions one needs to consider can be restricted by considering dominance ordering of partitions<sup>40</sup>.)

### STEP 3: Linear dependence of $b_n$ modes and restricted semi-standard tableaux

In steps 1 and 2 we have ignored the linear dependence of  $b_n$  expressed by the constraint  $\sum_n b_n = 0$ . Once linear dependence is taken into account, the states from Eq. (A16) still span,

$$\mathcal{V}_T = \text{span} \left\{ |\Sigma_t^\mu; \Theta_{st}^\mu\rangle \mid \begin{array}{l} \Sigma_t^\mu, \Theta_{st}^\mu \text{ semi-standard and} \\ \text{standard tableaux, } T = \sum_n t_n \end{array} \right\}. \quad (\text{A18})$$

However, they are linearly dependent in general. Fortunately, removing this linear dependence can be achieved by a harmless modification of our previous procedure. This modification consists of an additional restriction on the set of admissible semi-standard tableaux  $\Sigma_t^\mu$ . Specifically, we will show that restricting the semi-standard tableaux to the set

$$\mathcal{R}_T = \{ \Sigma_t^\mu \mid \Sigma_t^\mu \text{ has no "1" in its first row, } \sum_n t_n = T \}, \quad (\text{A19})$$

removes the linear dependence and

$$\mathcal{B}_T = \{ |\Sigma_t^\mu; \Theta_{st}^\mu\rangle \mid \Sigma_t^\mu \in \mathcal{R}_T, \Theta_{st}^\mu \text{ standard tableau} \} \quad (\text{A20})$$

forms a basis for  $\mathcal{V}_T$ . Furthermore, each subspace spanned by states with a fixed restricted semi-standard tableau  $\Sigma_t^\mu$  retains its character as an irreducible representation indexed by the partition  $(\mu)$ .

To prove this assertion, we first show that every state  $|\Sigma_t^{\mu'}; \Theta_{st}^{\mu'}\rangle$  obtained for a “forbidden” semi-standard-tableau  $\Sigma_t^{\mu'} \notin \mathcal{R}_T$  can be written as a linear combination of states  $|\Sigma_t^\mu; \Theta_{st}^\mu\rangle$  from the restricted set, i.e.  $\Sigma_t^\mu \in \mathcal{R}_T$ . Consider the vectors constructed in Eq. (A16) and note that the row-stabilizer can always be separated into the stabilizer of only the first row  $R_1$  and the stabilizer of all remaining rows  $R'$ :

$$\sum_{\tau \in R\Theta_{st}^\mu} \tau = \sum_{\tau' \in R'} \tau' \circ \sum_{\tau \in R_1} \tau. \quad (\text{A21})$$

*Example:* In this and all following examples we consider the “forbidden” state vector

$$\left| \begin{array}{|c|c|c|} \hline 0 & 1 & 2 \\ \hline 1 & 4 & \\ \hline \end{array} ; \begin{array}{|c|c|c|} \hline 1 & 3 & 5 \\ \hline 2 & 4 & \\ \hline \end{array} \right\rangle. \quad (\text{A22})$$

The stabilizer for row 1 consists of  $R_1 = \{e, (13), (15), (35), (135), (153)\}$ ; the stabilizer for the remaining rows is  $R' = \{e, (24)\}$ .

Proceeding with the decomposition of the “forbidden” state vector  $|\Sigma_t^{\mu'}; \Theta_{st}^\mu\rangle$  in terms of states with restricted semi-standard tableaux, let  $M = \{m_1, m_2, \dots, m_N\}$  denote the entries of the standard tableau  $\Theta_{st}^\mu$  (reading left to right, row by row), and  $M_1 = \{m_1, m_2, \dots, m_r\}$  the entries in row 1 only. Similarly, let  $(t_1, t_2, \dots, t_r)$  be the integer excitation numbers in the first row of the semi-standard tableau  $\Sigma_t^{\mu'}$  and (without loss of generality) assume that  $t_1 = \dots = t_{q-1} = 0$  and  $t_q = 1$  for  $q \leq r$ .

Next, we introduce the sets  $\Lambda_m = \{n_r, n_{r-1}, \dots, n_m\}$  and rewrite the stabilizer of row 1 as

$$\begin{aligned} & \sum_{\tau \in R_1} \tau \left[ b_{m_q}^\dagger b_{m_{q+1}}^{\dagger t_{q+1}} \dots b_{m_r}^{\dagger t_r} \right] \\ &= (q-1)! \sum_{n_r \in M_1} b_{n_r}^{\dagger t_r} \sum_{n_{r-1} \in M_1 \setminus \Lambda_r} b_{n_{r-1}}^{\dagger t_{r-1}} \dots \sum_{n_q \in M_1 \setminus \Lambda_{q+1}} b_{n_q}^\dagger. \end{aligned} \quad (\text{A23})$$

By construction, each successive sum over pseudo-mode indices  $n_r, n_{r-1}, \dots$  is associated with weakly decreasing excitation numbers  $t_r \geq t_{r-1} \geq \dots$  and the final sum over pseudo-mode indices  $n_q$  corresponds to case of a single excitation (entry “1” in row 1).

*Example:* Continuing with our previous example the above equality takes the form

$$\begin{aligned} & \sum_{\tau \in R_1} \tau \left( b_1^{\dagger 0} b_3^{\dagger 1} b_5^{\dagger 2} \right) = \sum_{n_3 \in \{1,3,5\}} b_{n_3}^{\dagger 2} \sum_{n_2 \in \{1,3,5\} \setminus \{n_3\}} b_{n_2}^\dagger \\ &= b_1^{\dagger 2} (b_3^\dagger + b_5^\dagger) + b_3^{\dagger 2} (b_1^\dagger + b_5^\dagger) + b_5^{\dagger 2} (b_3^\dagger + b_1^\dagger). \end{aligned}$$

Next, we use the linear dependence of the pseudo-modes to rewrite the final sum in Eq. (A23) as

$$\sum_{n_q \in M_1 \setminus \Lambda_{q+1}} b_{n_q}^\dagger = - \sum_{n \in \Lambda_{q+1}} b_n^\dagger - \sum_{n \in M \setminus M_1} b_n^\dagger. \quad (\text{A24})$$

The transformed expression has two separate sums over  $n$ : a sum over pseudo-modes that, according to Eq. (A23), are already occupied, and a sum over pseudo-modes in rows 2, 3,  $\dots$  of the standard tableau. The increase of excitation number produced by Eq. (A24) hence only affects pseudo-modes that are already occupied in Eq. (A23).

*Example:* Again continuing with our previous example we find

$$\sum_{n_2 \in \{1,3,5\} \setminus \{n_3\}} b_{n_2}^\dagger = - \sum_{n \in \{n_3\}} b_n^\dagger - \sum_{n \in \{2,4\}} b_n^\dagger. \quad (\text{A25})$$

Finally, we inspect the full state vector by using Eqs. (A21), (A23), and (A24). The terms resulting associated with a single index  $n$  [Eq. (A24)] can be re-expressed as a sum over the complete row stabilizer  $R$  and associated with a tableaux where the entry “1” in the first row of  $\Sigma_t^{\mu'}$  has been eliminated and another entry  $1 \leq t_n$  of  $\Sigma_t^{\mu'}$  has been increased by one: in such a way the state with “forbidden” semi-standard tableau

0	...	0	1	$t_{q+1}$	...	$t_r$
$t_{r+1}$	...	$t_{r_2}$				
$\vdots$						

is decomposed into a linear combination of states with tableaux

0	...	0	0	$t_{q+1}+1$	...	$t_r$
$t_{r+1}$	...	$t_{r_2}$				
$\vdots$						

0	...	0	0	$t_{q+1}$	...	$t_r+1$
$t_{r+1}$	...	$t_{r_2}$				
$\vdots$						

0	...	0	0	$t_{q+1}$	...	$t_r$
$t_{r+1}+1$	...	$t_{r_2}$				
$\vdots$						

0	...	0	0	$t_{q+1}$	...	$t_r$
$t_{r+1}$	...	$t_{r_2}+1$				
$\vdots$						

In cases where the above procedure results in a tableau that is not semi-standard, a straightening algorithm can be applied to generate the corresponding semi-standard tableau<sup>40</sup>, section 2.6. Importantly the straightening algorithm does not change the content of the tableaux and thus, does not change the fact that our procedure expresses the “forbidden” tableau in terms of semi-standard tableau with fewer “1” entries in row 1. Using this procedure, repeatedly if necessary, we can decompose

any state with “forbidden” semi-standard tableau as claimed. It is important, of course, that the removal of states occurs at the level of entire subspaces (indexed by the forbidden semi-standard tableaux) while the group action and hence the irreducibility of the remaining subspaces is unharmed.

*Example:* We complete our running example by decomposing the “forbidden” state vector

$$\left| \begin{array}{|c|c|c|} \hline 0 & 1 & 2 \\ \hline 1 & 4 & \\ \hline \end{array} ; \begin{array}{|c|c|c|} \hline 1 & 3 & 5 \\ \hline 2 & 4 & \\ \hline \end{array} \right\rangle. \quad (\text{A26})$$

in the restricted basis. Following our previous steps, the state vector can be expressed as

$$= \sum_{\sigma \in C} \sum_{\tau \in R'} \text{sgn}(\sigma) \sigma \tau \left[ b_2^\dagger b_4^{\dagger 4} \left( - \sum_{n_3 \in M_1} b_{n_3}^{\dagger 3} - \sum_{n_3 \in M_1} b_{n_3}^{\dagger 2} \sum_{n \in \{2,4\}} b_n^\dagger \right) \right]. \quad (\text{A27})$$

Together with a combinatorial factor (here:  $1/2$ ), the sums over  $n_3$  and  $\tau' \in R'$  can be recombined into the full row stabilizer:

$$= -\frac{1}{2} \sum_{\sigma \in C} \sum_{\tau \in R} \text{sgn}(\sigma) \sigma \tau \left[ b_2^\dagger b_4^{\dagger 4} \left( b_5^{\dagger 3} + b_5^{\dagger 2} \sum_{n \in \{2,4\}} b_n^\dagger \right) \right] \\ = -\frac{1}{2} \sum_{\sigma \in C} \sum_{\tau \in R} \text{sgn}(\sigma) \sigma \tau \left[ b_2^\dagger b_4^{\dagger 4} b_5^{\dagger 3} + b_2^\dagger b_4^{\dagger 4} b_5^{\dagger 2} \sum_{n \in \{2,4\}} b_n^\dagger + b_2^\dagger b_4^{\dagger 5} b_5^{\dagger 2} \right]$$

We have thus completed our goal of expressing the original “forbidden” state vector as a linear combination of the “restricted” state vectors

$$\left| \begin{array}{|c|c|c|} \hline 0 & 0 & 3 \\ \hline 1 & 4 & \\ \hline \end{array} ; \begin{array}{|c|c|c|} \hline 1 & 3 & 5 \\ \hline 2 & 4 & \\ \hline \end{array} \right\rangle, \left| \begin{array}{|c|c|c|} \hline 0 & 0 & 2 \\ \hline 2 & 4 & \\ \hline \end{array} ; \begin{array}{|c|c|c|} \hline 1 & 3 & 5 \\ \hline 2 & 4 & \\ \hline \end{array} \right\rangle, \left| \begin{array}{|c|c|c|} \hline 0 & 0 & 2 \\ \hline 1 & 5 & \\ \hline \end{array} ; \begin{array}{|c|c|c|} \hline 1 & 3 & 5 \\ \hline 2 & 4 & \\ \hline \end{array} \right\rangle.$$

With the decomposition of “forbidden” semi-standard tableaux in hand, we conclude by showing that the states  $|\Sigma_t^\mu; \Theta_{st}^\mu\rangle$  with restricted  $\Sigma_t^\mu \in \mathcal{R}_t^\mu$  not only span each  $V_\tau$  but are linearly independent. The proof is based on a simple dimensional argument. Counting the number of basis elements with  $T$  excitations, we find

$$\dim \mathcal{V}_\tau = \frac{(N-2+T)!}{T!(N-2)!}. \quad (\text{A28})$$

This should be compared with the dimensionality of subspaces constructed with restricted semi-standard tableaux  $\Sigma_t^\mu \in \mathcal{R}_t^\mu$ . For  $\sum_n t_n = T \leq 5$ , the explicit listing of restricted semi-standard tableaux is given in Table II. For comparison with Eq. (A28), note that the dimension  $d_\mu$  of the irreducible representation of  $S_N$  indexed by partition  $(\mu)$  can be obtained by the hook length formula, see Sagan<sup>40</sup>, section 3.10. We have verified that

$$\sum_{\Sigma_t^\mu \in \mathcal{R}_t^\mu} d_\mu = \frac{(N-2+T)!}{T!(N-2)!} \quad (\text{A29})$$

for all  $T \leq 5$ , and leave it as a conjecture that equality continues to hold for all higher  $T$ .

*Example:* As an example we consider  $T = 2$ . Using the hook-length formula the sum of the dimension of the irreducible subspaces indexed by the semi-standard tableaux

$$\left| \begin{array}{|c|c|c|c|} \hline 0 & \dots & 0 & 2 \\ \hline \end{array} \right\rangle, \left| \begin{array}{|c|c|c|} \hline 0 & \dots & 0 \\ \hline 2 & & \\ \hline \end{array} \right\rangle, \left| \begin{array}{|c|c|c|} \hline 0 & \dots & 0 \\ \hline 1 & 1 & \\ \hline \end{array} \right\rangle \quad (\text{A30})$$

is equal to  $1 + N - 1 + N(N-3)/2$ . Simple arithmetic shows this is equal to  $\dim \mathcal{V}_{T=2} = N(N-1)/2$  as expected.

In summary, the subspaces indexed by restricted semi-standard tableaux decompose each  $\mathcal{V}_\tau$  into its irreducible subspaces. As a final remark, we note that for  $T > 2$  multiplicities of irreducible representations can exceed 1. (Through  $T = 5$ , the largest multiplicity that occurs is 5, see Table II.) In such cases, the usual Gram-Schmidt procedure may be employed to generate orthogonal irreducible subspaces.

## Appendix B: Calculation of perturbative shifts according to irreducible subspaces

We next discuss the calculation of first-order shifts of energy levels in each irreducible subspace under the  $S_N$ -symmetric perturbation  $\delta H_U$ . In general, irreducible subspaces for the difference modes are labeled by restricted semi-standard tableaux. (For  $T \leq 2$ , is sufficient to specify  $T$  and the partition  $(\lambda)$  instead of full-blown semi-standard tableaux. In this appendix, we continue to employ the restricted semi-standard tableau notation.)

To calculate the first order shifts, we choose a unique element from each subspace. This is done by fixing a **reference standard tableau**  $\Theta_{\text{ref}}^\lambda$ , which we choose as the standard Young tableau of shape  $(\lambda)$  with entries 1 through  $N$  filled in column by column. Using this reference tableau, we obtain one representative state in each irreducible difference-mode subspace, which we denote by  $|\Sigma_t^\lambda\rangle$  ( $\Sigma_t^\lambda \in \mathcal{R}_t^\lambda$ ).

*Example:* The reference standard tableau for the partition  $(\lambda) = (N-2, 2)$  is

$$\Theta_{\text{ref}}^\lambda = \left| \begin{array}{|c|c|c|c|} \hline 1 & 3 & 5 & \dots & N \\ \hline 2 & 4 & & & \\ \hline \end{array} \right\rangle. \quad (\text{B1})$$

The state acting as the representative for the  $T = 2$ ,  $(\lambda) = (N-2, 2)$  subspace is then given by

$$\left| \begin{array}{|c|c|c|c|} \hline 0 & 0 & 0 & \dots & 0 \\ \hline 1 & 1 & & & \\ \hline \end{array} \right\rangle \sim \sum_{\sigma \in C} \sum_{\tau \in R} \text{sgn}(\sigma) \sigma \tau \left( b_2^\dagger b_4^\dagger \right) |0\rangle \\ \sim \left( b_2^\dagger - b_1^\dagger \right) \left( b_4^\dagger - b_3^\dagger \right) |0\rangle,$$

where the column and row stabilizers  $C$  and  $R$  are defined with respect to the reference standard tableau. With Eq. (A7), we obtain

$$\left\langle \begin{array}{|c|c|c|c|} \hline 0 & 0 & 0 & \dots & 0 \\ \hline 1 & 1 & & & \\ \hline \end{array} \right| \delta H_U \left| \begin{array}{|c|c|c|c|} \hline 0 & 0 & 0 & \dots & 0 \\ \hline 1 & 1 & & & \\ \hline \end{array} \right\rangle = 2E_C^a (1 - 1/N)$$

for the first-order shift of the irreducible subspace due to the effect of anharmonicity.

**Table II:** Irreducible subspaces for difference modes with total excitation number  $\tau \leq 5$ . In this table the equivalence class  $[t]$  with  $\lambda'_f$  pseudo-modes with exactly  $f$  excitations is denoted  $0^{\lambda'_0} 1^{\lambda'_1} \dots$  where all entries with  $\lambda'_f = 0$  are suppressed. All semi-standard tableau of shape  $(\mu)$  and content  $[t]$  are listed in the corresponding row and column.

T	$\begin{smallmatrix} [t] \\ 0^{\lambda_0} 1^{\lambda_1} \dots \end{smallmatrix}$	$(\mu) = (N)$	$(N-1, 1)$	$(N-2, 2)$	$(N-2, 1^2)$	$(N-3, 3)$	$(N-3, 2, 1^2)$	$(N-4, 4)$	$(N-4, 3, 1)$	$(N-5, 1^5)$
0	$0^N$	$\begin{smallmatrix} 0 & \dots & 0 \end{smallmatrix}$								
1	$0^{N-1} 1$		$\begin{smallmatrix} 0 & \dots & 0 \\ 1 \end{smallmatrix}$							
2	$0^{N-1} 2$	$\begin{smallmatrix} 0 & \dots & 0 & 2 \end{smallmatrix}$	$\begin{smallmatrix} 0 & \dots & 0 \\ 2 \end{smallmatrix}$							
	$0^{N-2} 1^2$			$\begin{smallmatrix} 0 & \dots & 0 \\ 1 & 1 \end{smallmatrix}$						
3	$0^{N-1} 3$	$\begin{smallmatrix} 0 & \dots & 0 & 3 \end{smallmatrix}$	$\begin{smallmatrix} 0 & \dots & 0 \\ 3 \end{smallmatrix}$							
	$0^{N-2} 12$		$\begin{smallmatrix} 0 & \dots & 0 & 2 \\ 1 \end{smallmatrix}$	$\begin{smallmatrix} 0 & \dots & 0 \\ 1 & 2 \end{smallmatrix}$	$\begin{smallmatrix} 0 & \dots & 0 \\ 1 \\ 2 \end{smallmatrix}$					
	$0^{N-3} 1^3$					$\begin{smallmatrix} 0 & 0 & \dots & 0 \\ 1 & 1 & 1 \end{smallmatrix}$				
4	$0^{N-1} 4$	$\begin{smallmatrix} 0 & \dots & 0 & 4 \end{smallmatrix}$	$\begin{smallmatrix} 0 & \dots & 0 \\ 4 \end{smallmatrix}$							
	$0^{N-2} 13$		$\begin{smallmatrix} 0 & \dots & 0 & 3 \\ 1 \end{smallmatrix}$	$\begin{smallmatrix} 0 & \dots & 0 \\ 1 & 3 \end{smallmatrix}$	$\begin{smallmatrix} 0 & \dots & 0 \\ 1 \\ 3 \end{smallmatrix}$					
	$0^{N-2} 2^2$	$\begin{smallmatrix} 0 & \dots & 0 & 2 & 2 \end{smallmatrix}$	$\begin{smallmatrix} 0 & \dots & 0 & 2 \\ 2 \end{smallmatrix}$	$\begin{smallmatrix} 0 & \dots & 0 \\ 2 & 2 \end{smallmatrix}$						
	$0^{N-3} 1^2 2$			$\begin{smallmatrix} 0 & \dots & 0 & 2 \\ 1 & 1 \end{smallmatrix}$		$\begin{smallmatrix} 0 & 0 & \dots & 0 \\ 1 & 1 & 2 \end{smallmatrix}$	$\begin{smallmatrix} 0 & \dots & 0 \\ 1 & 1 \\ 2 \end{smallmatrix}$			
	$0^{N-4} 1^4$							$\begin{smallmatrix} 0 & 0 & 0 & \dots & 0 \\ 1 & 1 & 1 & 1 \end{smallmatrix}$		
5	$0^{N-1} 5$	$\begin{smallmatrix} 0 & \dots & 0 & 5 \end{smallmatrix}$	$\begin{smallmatrix} 0 & \dots & 0 \\ 5 \end{smallmatrix}$							
	$0^{N-2} 14$		$\begin{smallmatrix} 0 & \dots & 0 & 4 \\ 1 \end{smallmatrix}$	$\begin{smallmatrix} 0 & \dots & 0 \\ 1 & 4 \end{smallmatrix}$	$\begin{smallmatrix} 0 & \dots & 0 \\ 1 \\ 4 \end{smallmatrix}$					
	$0^{N-2} 23$	$\begin{smallmatrix} 0 & \dots & 0 & 2 & 3 \end{smallmatrix}$	$\begin{smallmatrix} 0 & \dots & 0 & 3 \\ 2 \end{smallmatrix}$ $\begin{smallmatrix} 0 & \dots & 0 & 2 \\ 3 \end{smallmatrix}$	$\begin{smallmatrix} 0 & \dots & 0 \\ 2 & 3 \end{smallmatrix}$	$\begin{smallmatrix} 0 & \dots & 0 \\ 2 \\ 3 \end{smallmatrix}$					
	$0^{N-3} 1^2 3$			$\begin{smallmatrix} 0 & \dots & 0 & 3 \\ 1 & 1 \end{smallmatrix}$		$\begin{smallmatrix} 0 & 0 & \dots & 0 \\ 1 & 1 & 3 \end{smallmatrix}$	$\begin{smallmatrix} 0 & \dots & 0 \\ 1 & 1 \\ 3 \end{smallmatrix}$			
	$0^{N-3} 12^2$		$\begin{smallmatrix} 0 & \dots & 0 & 2 & 2 \\ 1 \end{smallmatrix}$	$\begin{smallmatrix} 0 & \dots & 0 & 2 \\ 1 & 2 \end{smallmatrix}$	$\begin{smallmatrix} 0 & \dots & 0 & 2 \\ 1 \\ 2 \end{smallmatrix}$	$\begin{smallmatrix} 0 & 0 & \dots & 0 \\ 1 & 2 & 2 \end{smallmatrix}$	$\begin{smallmatrix} 0 & \dots & 0 \\ 1 & 2 \\ 2 \end{smallmatrix}$			
	$0^{N-4} 1^3 2$					$\begin{smallmatrix} 0 & 0 & \dots & 0 & 2 \\ 1 & 1 & 1 \end{smallmatrix}$		$\begin{smallmatrix} 0 & 0 & 0 & \dots & 0 \\ 1 & 1 & 1 & 2 \end{smallmatrix}$	$\begin{smallmatrix} 0 & 0 & \dots & 0 \\ 1 & 1 & 1 \\ 2 \end{smallmatrix}$	
	$0^{N-5} 1^5$									$\begin{smallmatrix} 0 & 0 & 0 & 0 & \dots & 0 \\ 1 & 1 & 1 & 1 & 1 \end{smallmatrix}$

### Appendix C: Lagrangian for superinductance and difference mode variables

After transforming to superinductance and difference mode variables, the Lagrangian of Eq. (1) can be cast into the form

$$\mathcal{L}_{\text{SFM}} = \frac{\hbar^2}{16E_C^b} \dot{\phi}^2 + \frac{\hbar^2}{16E_C^a} \sum_{\mu} \dot{\xi}_{\mu}^2 + E_J^b \cos(\phi + \varphi_{\text{ext}}) + E_J^a \sum_m \cos \left[ \phi/N + \sum_{\mu} W_{\mu m} \xi_{\mu} \right]. \quad (\text{C1})$$

This expression for the Lagrangian has important advantages over its equivalent form expressed in terms of  $\theta_m$ . First, the kinetic energy is now *diagonal*. Second, low-energy minima of the potential energy  $U$  are in locations where each difference mode variable vanishes,  $\xi_{\mu} = 0$ . Third, fluctuations between minima are dominantly described by the  $\phi$  variable. The ability to simultaneously expand around  $\xi_{\mu} = 0$  for each local minimum of  $U$  is key in the derivation of the superinductance model used previously<sup>8,9</sup>.

### Appendix D: Incorporating capacitances to ground

The  $(N + 1)$  node variables  $\varphi_j$  can be expressed in terms of the  $N$  junction variables  $\theta_m$  when using the constraint that the total charge  $\sum_j n_j$  of all superconducting islands be zero. To see this, we may use  $\tau = \varphi_0$  as a reference variable and express every other node variable  $\varphi_j$  ( $j = 1, \dots, N$ ) as

$$\varphi_j = \tau - \frac{j}{N} \varphi_{\text{ext}} + \sum_{m=1}^j \theta_m. \quad (\text{D1})$$

Note that  $\dot{\tau} \Phi_0 / 2\pi$  represents a uniform voltage shift of all superconducting islands relative to ground, and that  $\tau$  is cyclic, i.e., the Lagrangian is independent of  $\tau$ . Hence, its conjugate momentum is conserved:  $\partial \mathcal{L} / \partial \dot{\tau} = \text{const}$ . This constant of motion, in fact, corresponds to the total charge  $n_{\text{tot}}$  since

$$\frac{\partial \mathcal{L}}{\partial \dot{\tau}} = \sum_j \frac{\partial \varphi_j}{\partial \tau} \frac{\partial \mathcal{L}}{\partial \dot{\varphi}_j} = \sum_j n_j = n_{\text{tot}}. \quad (\text{D2})$$

Imposing the constraint  $n_{\text{tot}} = 0$  thus allows us to eliminate  $\dot{\tau}$  from the Lagrangian, and to work with a Lagrangian (strictly speaking, a Routhian) which only depends on  $\theta_m$  and  $\dot{\theta}_m$ . Using this procedure the contribution to the kinetic energy due to ground capacitances  $\frac{1}{2} (\Phi_0 / 2\pi)^2 \sum_{i=0}^N C_{gi} \dot{\varphi}_i^2$  in Eq. (1) takes the form  $\frac{1}{2} \sum_{mn} \mathcal{G}_{mn} \dot{\theta}_m \dot{\theta}_n$  where

$$\mathcal{G}_{mn} = \frac{(\Phi_0 / 2\pi)^2}{\sum_{i=0}^N C_{gi}} \sum_{i=0}^{\min\{m,n\}-1} \sum_{j=\max\{m,n\}}^N C_{gi} C_{gj}. \quad (\text{D3})$$

Then, assuming the two large superconducting islands surrounding the black sheep junction have ground capacitance

$C_g^b = e^2 / 2E_g^b$  while the ground capacitance of the remaining small array islands are  $C_g^a = e^2 / 2E_g^a$ , and using the variables  $\xi_{\mu}$  defined in Eq. (3) the kinetic energy terms of the Lagrangian [Eq. (1)] takes the form

$$\frac{\hbar^2}{16} \sum_{\mu, \nu=0}^{N-1} (M_{\mu\nu} + G_{\mu\nu}) \dot{\xi}_{\mu} \dot{\xi}_{\nu}. \quad (\text{D4})$$

Here for compactness we use the shorthand  $\xi_0 = \phi$ . The symmetric  $N \times N$ -matrices  $M$  and  $G$  have the following form:

$$M_{00} = 1/E_C^b, \quad M_{0\mu} = 0, \quad M_{\mu\nu} = \delta_{\mu\nu} / E_C^a \quad (\text{D5})$$

and

$$G_{00} = \frac{1}{2E_g^b} + \frac{(N-1)(N-2)}{12NE_g^a}, \quad (\text{D6})$$

$$G_{0\mu} = \frac{o_{\mu+1} c(\mu)}{2E_g^a \sqrt{2N} s(\mu)^2}$$

$$G_{\mu\nu} = \frac{\delta_{\mu\nu}}{4E_g^a s(\mu)^2}$$

$$+ \frac{E_g^b o_{\mu} o_{\nu} c(\mu) c(\nu)}{NE_g^a [2 + (N-1)E_g^b / E_g^a] s(\mu)^2 s(\nu)^2},$$

where  $c(\mu)$  and  $s(\mu)$  are shorthand for  $\cos(\pi\mu/2N)$  and  $\sin(\pi\mu/2N)$ , respectively. Furthermore, the coefficient  $o_{\mu}$  is 1 whenever the index  $\mu$  is an odd integer, and zero otherwise.

Performing the Legendre transform, the perturbation from ground capacitances takes the form

$$\delta H_C = 4 \sum_{\mu, \nu=0}^{N-1} [(M + G)^{-1} - M^{-1}]_{\mu\nu} \partial_{\xi_{\mu}} \partial_{\xi_{\nu}}. \quad (\text{D7})$$

For small ground capacitances, the entries of  $G$  are small compared to those of  $M$  and we approximate  $(M + G)^{-1} \simeq M^{-1} - M^{-1} G M^{-1}$ , which yields equation (7) in the main text.

### Appendix E: Limits of the perturbative approach

Corrections in the main text are treated perturbatively and we briefly comment on necessary conditions for this approach to be valid. First, we remark that the energy scales  $\delta E_J^{\text{sd}}$  and  $\delta E_C^{\text{sd}}$  of Eqs. (11) and (12) must remain sufficiently small relative to the typical energy scales of the superinductance spectrum. Secondly, when the magnitude of  $\langle 0 | \delta H_C^d | (N) 2 \rangle$  or  $\langle 0 | \delta H_C^d (a_1^{\dagger})^2 | 0 \rangle$  becomes of order  $2\Omega$ , the ground state of the difference will require non-perturbative corrections. To prevent this, the respective inequalities

$$\sqrt{N/2} \ll 16/\Delta_{\xi}^2, \quad (N\Delta_{\xi}/2\pi)^2 \ll E_g^a/E_C^a \quad (\text{E1})$$

must hold. Thus to connect with the  $N \rightarrow \infty$  limit (see, e.g., Ref. 38) a different approximation scheme to model the low energy spectrum of fluxonium may become necessary. However, in the case of the fluxonium samples previously studied in Refs. 8,9, the range of validity of the perturbative approach is well satisfied.



## Appendix F: Parameter values used in numerical calculations

The specific parameters used in all calculations in the main text are  $N = 43$ ,  $E_C^a = 1.0$ ,  $E_J^a = 26.4$ ,  $E_C^b = 3.8$ ,  $E_J^b = 8.9$ ,  $\delta E_J = 0.15$ ,  $E_g^b = 5$  and  $E_g^a = 250$ . Using Eqs. (8) these parameters yield  $E_C^{\text{si}} = 2.5$  and  $E_L = 0.53$ ; all energies in units of  $\hbar$  GHz.